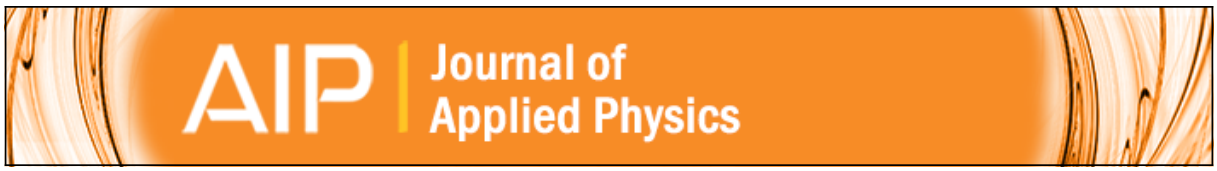

Optimized amorphous silicon oxide buffer layers for silicon heterojunction solar cells with microcrystalline silicon oxide contact layers

Kaining Ding, Urs Aeberhard, Friedhelm Finger, and Uwe Rau

Citation: Journal of Applied Physics **113**, 134501 (2013); doi: 10.1063/1.4798603
View online: http://dx.doi.org/10.1063/1.4798603
View Table of Contents: http://scitation.aip.org/content/aip/journal/jap/113/13?ver=pdfcov
Published by the AIP Publishing

Optimized amorphous silicon oxide buffer layers for silicon heterojunction solar cells with microcrystalline silicon oxide contact layers

Kaining Ding,[a] Urs Aeberhard, Friedhelm Finger, and Uwe Rau
IEK5-Photovoltaik, Forschungszentrum Jülich, Leo-Brandt-Strasse, 52425 Jülich, Germany

(Received 16 November 2012; accepted 15 March 2013; published online 1 April 2013)

We report on the systematic optimization of the intrinsic amorphous silicon oxide buffer layer in interplay with doped microcrystalline silicon oxide contact layers for silicon heterojunction solar cells using all silicon oxide based functional layers on flat p-type float-zone wafers. While the surface passivation quality is comparably good within a wide range of low oxygen contents, the optical band gap increases and the dark conductivity decreases with increasing oxygen content, giving rise to an inevitable trade-off between optical transparency and electrical conductivity. On the cell level, fill factor FF and short circuit current density J_{sc} losses compete with the open circuit voltage V_{oc} gains resulting from a thickness increase of the front buffer layers, whereas J_{sc} and V_{oc} gains compete with FF losses resulting from increasing thickness of the rear buffer layers. We obtained the highest active area efficiency of $\eta_{act} = 18.5\%$ with $V_{oc} = 664\,mV$, $J_{sc} = 35.7\,mA/cm^2$, and $FF = 78.0\%$ using 4 nm front and 8 nm rear buffer layer with an oxygen content of 5%. © *2013 American Institute of Physics*. [http://dx.doi.org/10.1063/1.4798603]

I. INTRODUCTION

Silicon heterojunction (SHJ) solar cells with thin intrinsic buffer layers[1] provide numerous advantages as compared to conventional c-Si technology, e.g., simple and low temperature process, good surface passivation,[2] processability of very thin wafers, and a high energy conversion efficiency with a low temperature coefficient.[3,4] Intrinsic amorphous silicon oxide (a-SiO_x:H) shows good surface passivation properties and, as compared to a-Si:H, higher optical band gap, higher thermal stability,[5] and suppression of epitaxial growth.[6,7] Doped microcrystalline silicon oxide (μc-SiO_x:H) has been partially implemented as emitter or back surface field (BSF) material in SHJ solar cells due to its beneficial optical properties combined with high electrical conductivities.[8,9] Recently, an all-SiO_x SHJ solar cell has been introduced with all silicon oxide based buffer and contact layers using μc-SiO_x:H ⟨n⟩ emitter, μc-SiO_x:H ⟨p+⟩ BSF, and a-SiO_x:H ⟨i⟩ buffer layers.[10] A similar device structure has been reported by Rattanapan *et al.*,[11] where the authors investigated the applicability of p-type μc-SiOx:H as a passivating BSF in flat p-type SHJ solar cells and demonstrated efficiency values up to 18.5% on SHJ solar cells without a rear buffer layer.

The present work provides a systematic study on the material and device development of the a-SiO_x:H ⟨i⟩ buffer layers for SHJ solar cells with all functional layers based on SiO_x. In particular, we investigated the structural, optoelectronic, and passivation properties of a-SiO_x:H ⟨i⟩ layers and systematically optimized the buffer layer thicknesses with respect to the solar cell efficiency. As a result, we can clearly identify competing effects resulting from increasing/decreasing front and rear buffer layer thickness. For the front side, increasing the buffer thickness leads to a higher series resistance (and correspondingly lower fill factor FF) and higher parasitic absorption (lower short circuit current density J_{sc}) on the one hand, and a lower front interface recombination rate (lower open circuit voltage V_{oc}) on the other hand. For the rear side, a thicker buffer layer leads to an improved rear interface passivation (resulting in higher V_{oc} and higher J_{sc}) but an increased series resistance (lower FF) similar as in conventional a-Si:H heterojunction back contacts.[12]

II. EXPERIMENTAL

All a-SiO_x:H ⟨i⟩, μc-SiO_x:H ⟨n⟩, and μc-SiOx:H ⟨p+⟩ layers were deposited using plasma enhanced chemical vapour deposition (PECVD) with SiH_4, CO_2, H_2 as process gases and PH_3 or $B(CH_3)_3$ as doping gases. The most important deposition parameters are listed in Table I. We fabricated a-SiO_x:H ⟨i⟩ single layers with varying CO_2 gas flow rates on glass substrates for the determination of the layer properties and samples for lifetime measurements on double side polished, ⟨100⟩ orientated, 250 μm thick p-type float zone silicon wafers with a resistivity of $3.2 \pm 0.1\,\Omega\,cm$. Prior to deposition, the wafers were treated in a mixture of sulphuric acid and hydrogen peroxide to clean off organic residues, followed by a dipping in diluted hydrofluoric acid to remove the native oxide from the wafer surface. The lifetime samples consist of a-SiO_x:H ⟨i⟩ single layers with various CO_2 flow rates and layer thicknesses as well as a-SiO_x:H ⟨i⟩/μc-SiO_x:H ⟨n⟩ double layers with varying i-layer thickness (inset Fig. 3). SHJ solar cells were fabricated on c-Si ⟨p⟩ wafers with the same specification and cleaning procedure as the wafers used for lifetime measurements. Figure 1 sketches the structure of the SHJ solar cell. In this study, only the front and rear a-SiO_x:H ⟨i⟩ buffer layer thicknesses were varied. The thicknesses were estimated from deposition times and the pre-determined deposition rate. As transparent conducting oxide (TCO), we used sputtered ITO and as metal contact silver grids thermally evaporated through a shadow

[a]Author to whom correspondence should be addressed. Electronic mail: k.ding@fz-juelich.de. Tel.: +49 (0)2461 611604. Fax: +49 (0)2461 613735.

TABLE I. Deposition conditions of different PECVD silicon oxide films, where T_{sub} is the substrate temperature, p is the deposition pressure, P is the power density, and f is the deposition frequency. The gas flow ratios are defined as $r_{CO2}=f_{CO2}/(f_{CO2}+f_{SiH4})$, $r_{doping}=f_{doping}/(f_{doping}+f_{SiH4})$, $r_H=f_H/f_{total}$, where f denotes the flow rates of the gases.

Film type	$r_{CO2}/r_{doping}/r_H/f_H$ [(%)/(%)/(%)/(sccm)]	$T_{sub}/p/P/f$ [(°C)/(mbar)/(mW/cm^2)/(MHz)]
a-SiO$_x$ ⟨i⟩	10–50/0/50/10	200/0.25/17/81.40
μc-SiO$_x$ ⟨n⟩	30/2.0/99.5/500	200/4.00/337/13.56
μc-SiO$_x$ ⟨p⟩	20/0.5/99.5/500	200/4.00/337/13.56

mask (active area = 0.67 cm^2) on the front side and full area silver on the rear side. As a final step, the complete device was annealed on a heating plate at 200 °C for 2 min for the contact forming and the improvement of the passivation quality.

The oxygen content c_O of the a-SiO$_x$:H ⟨i⟩ single layers was determined using Rutherford backscattering spectrometry. The E_{04} gap energy, i.e., the energy at which the absorption coefficient amounts to 10^4 cm^{-1} and which here is determined from photo-thermal deflection spectroscopy, is taken as a measure for the optical band gap. The dark conductivity σ_{dark} was measured at room temperature in vacuum between two coplanar silver contacts with 0.5 mm inter-electrode gap. The effective carrier lifetime τ_{eff} was measured with a commercial quasi steady state photo conductance (QSSPC) measurement setup. The τ_{eff} values at the light intensity of 1 sun are converted into an implied open circuit voltage $V_{oc,imp}$ as a measure for the interface passivation quality.[13] A double source (class A) AM 1.5 solar simulator was used to determine the cell efficiencies η at standard test conditions (AM1.5 G, 100 mW/cm^2, 25 °C), as well as fill factors FF, open circuit voltages V_{oc}, and short circuit current densities J_{sc}. The external quantum efficiency, EQE, was measured in a differential spectral response (DSR) setup by positioning a focused light spot between two silver grids. The integrated short-circuit current density $J_{sc,int}$ was determined by integrating the product of EQE and AM 1.5 G solar spectrum over the wavelength range from 300 nm to 1150 nm. Considering $J_{sc,int}$ from DSR being more accurate than J_{sc} from the solar simulator, we recalculated the efficiency η_{act} of the active area from FF, V_{oc}, and $J_{sc,int}$. The internal quantum efficiency, IQE, was determined from the equation $IQE = EQE/(1-R)$, where R is the cell reflectance measured with a commercial optical spectrometer.

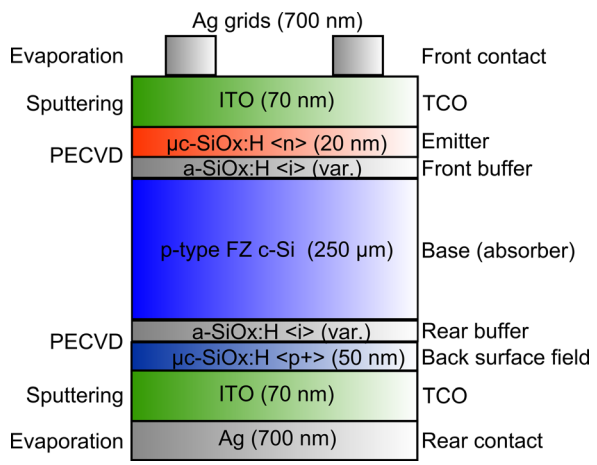

FIG. 1. Schematic illustration of the SHJ solar cell structure with PECVD grown emitter, BSF, and buffer layers on flat p-type wafer covered with sputtered TCO and thermally evaporated silver.

III. RESULTS

Figure 2 displays the oxygen content c_O, the optical band gap E_{04}, and the dark conductivity σ_{dark} plotted versus the CO_2 gas flow ratio $r_{CO2}=f_{CO2}/(f_{CO2}+f_{SiH4})$ used during the deposition of the a-SiOx:H ⟨i⟩ films, where f_{CO2} and f_{SiH4} are the CO_2 and SiH_4 gas flow rates, respectively. As the r_{CO2} increases from 10% to 50%, the c_O increases linearly from 1.6% to 10.0%. The E_{04} band gap shifts from 2.0 eV to higher energies up to 2.2 eV, and the σ_{dark} reduces by almost two orders of magnitude from 1.3×10^{-10} S/cm to 3.9×10^{-12} S/cm. Figure 3(a) shows the implied open circuit voltage $V_{oc,imp}$ plotted versus c_O for the lifetime samples with a-SiOx:H ⟨i⟩ single layers. The $V_{oc,imp}$ decreases slightly with increasing c_O, however, remains at around 720 mV up to $c_O = 10.0\%$. Figure 3(b) displays the $V_{oc,imp}$ as a function of the a-SiOx:H ⟨i⟩ thickness $d_{a\text{-}SiOx:H\ \langle i\rangle}$ for the lifetime samples with a-SiOx:H ⟨i⟩ single layers and a-SiOx:H ⟨i⟩/μc-SiOx ⟨n⟩ double layers. For these series, all a-SiOx:H ⟨i⟩ layers were deposited with a r_{CO2} of 30% corresponding to a c_O of 5.0%. In general, the $V_{oc,imp}$ decreases with decreasing $d_{a\text{-}SiOx:H\ \langle i\rangle}$, whereas an increase of

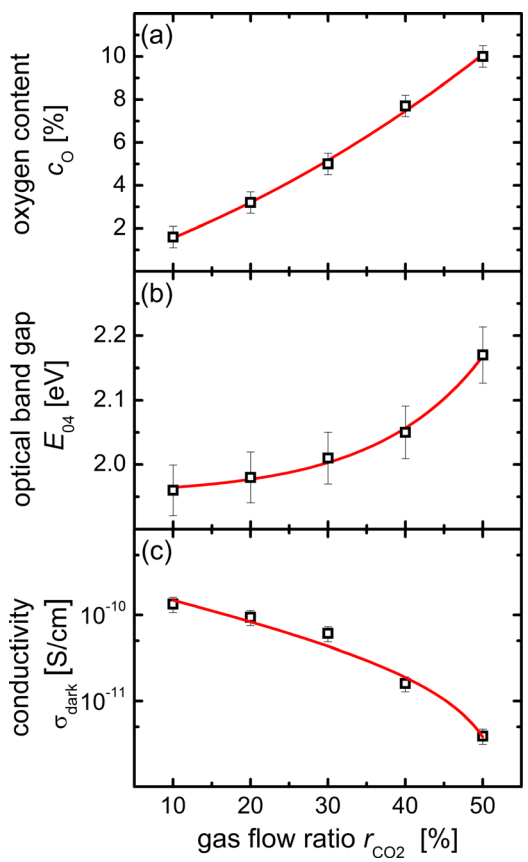

FIG. 2. Oxygen content c_O (a), optical band gap E_{04} (b), and dark conductivity σ_{dark} (c) versus the CO_2 gas flow ratio r_{CO2} for a-SiO$_x$:H ⟨i⟩ layers.

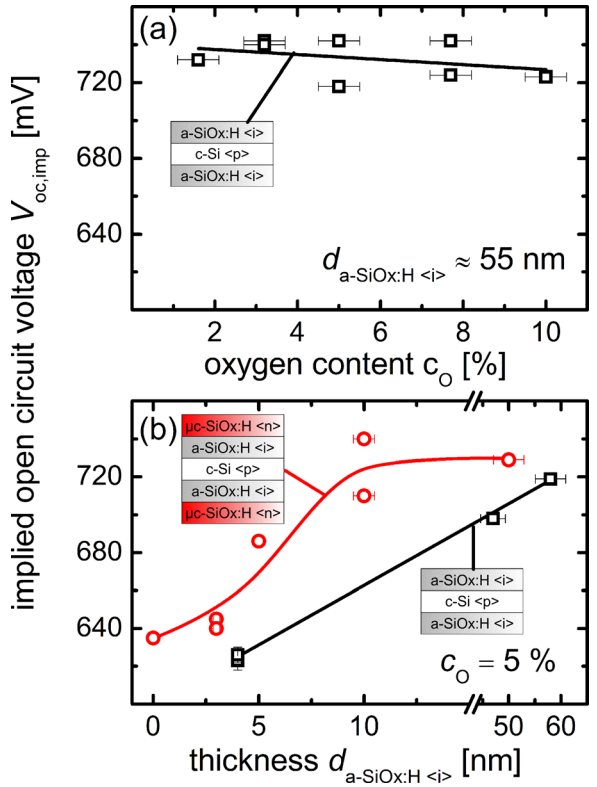

FIG. 3. Implied open circuit voltage $V_{oc,\ imp}$ versus (a) oxygen content c_O for a-SiO_x:H ⟨i⟩ lifetime samples and (b) thickness $d_{a\text{-}SiOx:H\ ⟨i⟩}$ for a-SiO_x:H ⟨i⟩ and a-SiO_x:H ⟨i⟩/µc-SiO_x ⟨n⟩ lifetime samples. The insets illustrate the schematic cross-sectional structure of the respective sample series.

the $V_{oc,imp}$ is observed as the additional µc-SiO_x:H ⟨n⟩ layer is deposited onto the a-SiO_x:H ⟨i⟩ layer. The $V_{oc,imp}$ seems to saturate at around 730 mV at 10 nm for a-SiOx:H ⟨i⟩/µc-SiOx ⟨n⟩ double layers.

Figure 4 displays the solar cell parameters plotted versus the rear buffer layer thicknesses for three different SHJ solar cell series each with the front buffer layer thickness d_{front} kept at the same size (1), half the size (1/2), or a third of the size (1/3) of that of the rear buffer layer thickness d_{rear}. Within each series, the open circuit voltage V_{oc} and the short circuit current density $J_{sc,int}$ increase with thicker buffer layers, whereas the fill factor *FF*, first remaining at a high value showing only slight deterioration with thickness, decreases strongly upon a critical rear buffer thickness. Thus, the efficiency η_{act} first increases with increasing buffer layer thickness due to the increase in V_{oc} and $J_{sc,int}$, but then decreases due to significant loss in *FF*. Comparison between the series (1) and (1/2) shows a decrease in V_{oc} and an increase in $J_{sc,int}$ as the d_{front} is reduced. The critical rear buffer thickness, upon which the *FF* starts to strongly deteriorate, shifts to higher d_{rear} values. Consequently, the maximum η_{act} increases and shifts to thicker rear buffer layers with thinner front buffer layers for the series (1) and (1/2). In comparing the series (1/2) and (1/3), it is found that the decrease in V_{oc} and the increase in $J_{sc,int}$ continue with further reduction of the d_{front}. However, no significant change in the *FF* was observed for these two series. Since the loss in V_{oc} and the gain in $J_{sc,int}$ compensate each other, the η_{act} as a function of the d_{rear} was similar for the series (1/2) and (1/3). The highest efficiency was obtained for the 4.0 nm front and 8.0 nm rear buffer layer thickness SHJ solar cell of the (1/2) series with $V_{oc} = 664$ mV, $J_{sc,int} = 35.7$ mA/cm^2, $FF = 78.0\%$, and $\eta_{act} = 18.5\%$.

Figure 5 shows the *IQE* of the SHJ solar cells with different d_{front} and d_{rear} measured at a bias voltage of 0 V. Figure 5(a) compares the *IQE* of two cells with same d_{front} but different d_{rear}, showing an increase of the carrier extraction especially in the long wavelength range with increasing d_{rear}. Figure 5(b) compares the *IQE* of three cells with same d_{rear} but different d_{front}, showing a decrease of the carrier extraction over the whole spectral range with increasing d_{front}.

IV. DISCUSSIONS

The linear increase of the oxygen content with increasing r_{CO2} reveals that the oxygen atoms, which were produced during the cracking process of CO_2 into CO and O by the plasma, are incorporated into the material proportional to the CO_2 gas flow. Secondary ion mass spectrometry results show

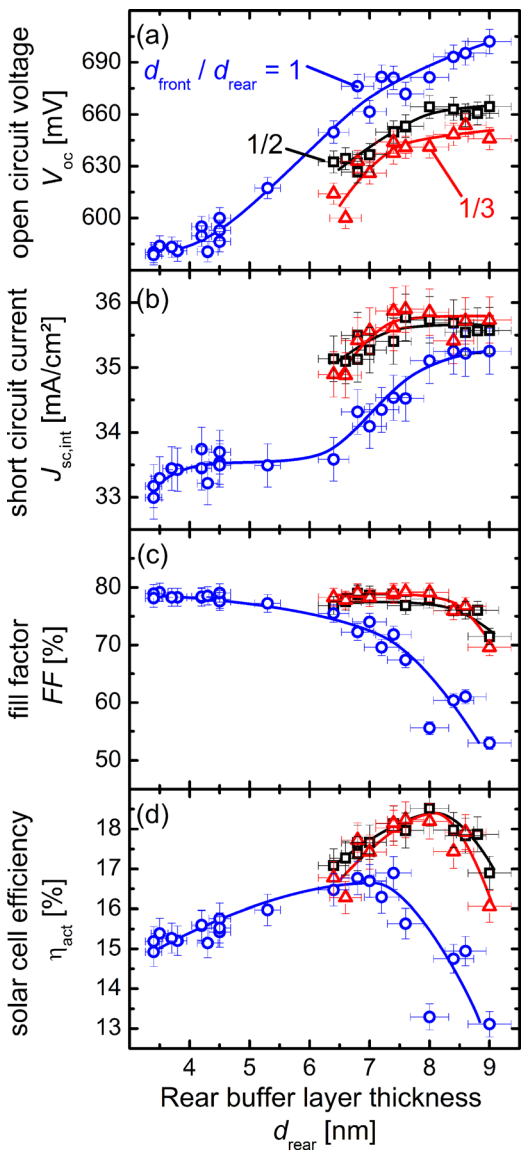

FIG. 4. Dependence of the SHJ solar cell parameters on the thickness of the rear a-SiO_x:H ⟨i⟩ buffer layer for fixed thickness ratios.

that less than 0.1% carbon atoms were embedded into the material, which is not surprising, since the C-O bond has high bonding energy and is thus unlikely to be cracked by the plasma.[14] All a-SiO_x:H ⟨i⟩ samples consist of an amorphous phase only, which was checked with Raman spectroscopy. We decided to use the $c_O = 5.0\%$ a-SiO_x:H ⟨i⟩ with an reasonable trade-off between optical transparency ($E_{04} = 2.0$ eV) and electrical conductivity ($\sigma_{dark} = 6 \times 10^{-11}$ S/cm) for implementation as buffer layer in our SHJ solar cells, since the passivation quality of the a-SiO_x:H ⟨i⟩ layers with c_O in the range of 1.6%–10.0% is comparably good.

The passivation quality of the $c_O = 5.0\%$ a-SiO_x:H ⟨i⟩ lifetime samples decreases as its thickness is reduced, which we attribute to an increased probability of charge carriers to tunnel through the a-SiO_x:H ⟨i⟩ layer and recombine via defect states at the a-SiO_x:H/air interface.[10] The passivation quality is improved for the same i-layer thickness by inserting an additional μc-SiO_x ⟨n⟩ layer on top of the a-SiO_x:H ⟨i⟩ (Fig. 3(b)), which is likely due to the built-in electrical field that reflects the majority holes in the c-Si bulk from the heterojunction interface.[15] However, the $V_{oc,imp}$ saturates at around 730 mV at an i-layer thickness of 10 nm, indicating that the $V_{oc,imp}$ is no more limited by interface recombination beyond this i-layer thickness.[16]

Comparison between the solar cell series (1), (1/2), and (1/3) shows that the V_{oc} increases with thicker d_{front} at constant d_{rear} (Fig. 4(a)), which can be attributed to improved front interface passivation in consistency with the QSSPC results. At the same time, the $J_{sc,int}$ decreases with thicker d_{front} (Fig. 4(b)), which can be assigned to higher parasitic absorption losses from the front buffer layer and supported by the slightly decreasing IQE in the short wavelength range with increasing d_{front} as shown in Figure 5(b) and confirmed by device simulation using AFORS-HET (not shown).[17]

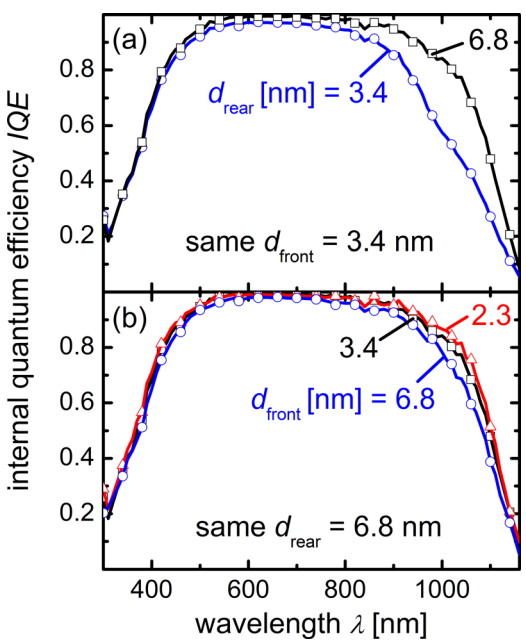

FIG. 5. Internal quantum efficiency of the SHJ solar cells with different front and rear a-SiO_x:H ⟨i⟩ buffer layer thicknesses measured at the bias voltage of 0 V.

However, the simulation results do not show any change of IQE in the long wavelength range with varying d_{front}. This disagreement with the experimental observation will be explained below. Device simulation also reveals that a reduced front interface passivation does not deteriorate $J_{sc,int}$, since the pronounced band bending at the emitter (n)/base (p) interface in the short circuit case effectively reflects majority holes and extracts minority electrons close to this interface before the charge carriers recombine at the heterojunction interface. In difference to the situation at the front interface, the rear interface passivation will likely affect the IQE in the long wavelength range due to the weaker band bending at the base (p)/BSF (p+) interface as compared to the emitter (n)/base (p) interface in the short circuit case. In order to verify this assumption, we analysed the effect of varying d_{rear} at constant d_{front} by comparing the solar cells with $d_{rear} = 3.0$ nm–4.5 nm from the series (1) with those with $d_{rear} = 6.0$ nm–9.0 nm from the series (1/2). With thicker d_{rear} at constant d_{front}, V_{oc} (Fig. 4(a)) and $J_{sc,int}$ (Fig. 4(b)) increase significantly, which can be attributed to the reduction of the rear interface recombination. This is consistent with the comparison of the IQE of two SHJ cells with the same d_{front} but different d_{rear} (Fig. 5(a)), showing strong increase of the carrier extraction especially in the long wavelength range with increasing d_{rear}. Therefore, we attribute the noticeable change of the IQE in the long wavelength range for SHJ solar cells with thicker d_{front} at constant d_{rear} (Fig. 5(b)) to the small thickness variation of d_{rear} within the error bars as indicated in Fig. 4(b).

The higher *FF* (Fig. 4(c)) with thinner d_{front} and d_{rear} can be assigned to the lower series resistance of the buffer layers, which overcompensates the deterioration of the *FF* due to reduced interface recombination by reducing the thickness of the buffer layers as reported in the Ref. 18. Within each series, the *FF* first remains on a high value before it decreases beyond a critical buffer layer thickness combination due to increased series resistance. However, the *FF* does not exceed the value of 78% with varying buffer layer thicknesses for all three series, which is an indication for the limitation of the *FF* by other sources of series resistance, e.g., the Ag/ITO, ITO/μc-SiO_x:H contact resistances, or the series resistance of the ITO or the μc-SiO_x:H layers.

It is worthwhile to note that the V_{oc} values of the highest efficiency solar cells from Ref. 11 (659 mV) and this work (664 mV) are similar, even though a rear buffer layer is omitted in Ref. 11. This strongly indicates that our μc-SiOx:H ⟨p⟩ BSF still needs to be optimized in terms of a lower defect density required for well passivated a-SiO_x:H ⟨i⟩/μc-SiO_x:H ⟨p⟩ interface and/or a higher doping concentration required for efficient electron reflexion. In addition, the deposition of a-Si:H ⟨p+⟩ film on a-Si:H ⟨i⟩ layer is known to cause the deterioration of surface passivation quality due to lowered Si-H bond rupture energies in the a-Si:H ⟨p+⟩ and the underlying a-Si:H ⟨i⟩ layers,[19] which might also occur during the deposition of μc-SiOx:H ⟨p⟩ film on a-SiO_x:H ⟨i⟩ layer and thus limits the V_{oc} of the SHJ solar cells in this work. However, this assumption has to be reappraised by the passivation quality of a-SiO_x:H ⟨i⟩/μc-SiO_x ⟨p⟩ double layers in comparison with that of a-SiO_x:H ⟨i⟩ single layers. The

optimization of the μc-SiO$_x$:H $\langle$p$\rangle$ BSF as well as the verification of the a-SiO$_x$:H $\langle$i$\rangle$/μc-SiO$_x$ $\langle$p$\rangle$ passivation quality will be targeted in future works.

V. CONCLUSIONS

We used $c_O = 5\%$ a-SiO$_x$:H $\langle$i$\rangle$ with good passivation property and a reasonable compromise between optical transparency and electrical conductivity as a buffer layer material in our SHJ solar cells. Under the precondition that the thickness combination of both buffer layers is small enough to maintain a high FF, the thickness of the rear buffer layer should be as large as possible to passivate the rear heterojunction interface, in order to guarantee high V_{oc} and J_{sc}, whereas the front buffer layer should have a thickness with the optimum trade-off between front heterojunction interface passivation (V_{oc}) and parasitic absorption loss (J_{sc}). The optimum combination of both buffer layer thicknesses, which leads to the highest efficiency, was 4 nm for the front buffer and 8 nm for the rear buffer layer. Yet without optimization of the μc-SiO$_x$:H $\langle$n$\rangle$ emitter and μc-SiO$_x$:H $\langle$p+$\rangle$ BSF, we obtained the highest efficiency of $\eta_{act} = 18.5\%$ with $V_{oc} = 664$ mV, $J_{sc,int} = 35.7$ mA/cm^2, and $FF = 78.0\%$.

ACKNOWLEDGMENTS

The authors thank J. Klomfaß for PDS measurements, B. Holländer for RBS measurements, J. Hotovy for ITO sputtering, and F. Einsele for his groundwork in c-Si passivation using a-SiO$_x$:H $\langle$i$\rangle$ layers. Financial support was provided by the German Federal Ministry of Education and Research (BMBF) under Grant No. 03SF0352E.

[1]T. Kinoshita, D. Fujishima, A. Yano, A. Ogane, S. Tohoda, K. Matsuyama *et al.*, "The approaches for high efficiency HIT solar cell with very thin (<100 μm) silicon wafer over 23%," in *Proceedings of the 26th European Photovoltaic Solar Energy Conference, Hamburg, Germany, 5-9 Sep 2011* (WIP, 2011), pp. 871–874.

[2]A. M. Froitzheim, M. L. D. Scherff, A. Ulyashin, O. Milch, M. Schmidt, W. R. Fahrner *et al.*, "Amorphous/crystalline silicon heterojunction solar cells with intrinsic buffer layer," in *Proceedings of the 3rd World Conference on Photovoltaic Energy Conversion, Osaka, Japan, 11-18 May 2003*, edited by W. Kurokawa, K. Kazmerski, L. L. McNelis, B. Yamaguchi, M. Wronski, and C. Sinke (WIP, 2003), pp. 180–183.

[3]J. Damon-Lacoste, P. R. i Cabarrocas, P. Chatterjee, Y. Veschetti, A. S. Gudovskikh, J. P. Kleider *et al.*, "About the efficiency limits of heterojunction solar cells," J. Non-Cryst. Solids **352**, 1928–1932 (2006).

[4]S. De Wolf, A. Descoeudres, Z. C. Holman, and C. Ballif, "High-efficiency silicon heterojunction solar cells: A review," Green **2**, 7–24 (2012).

[5]F. Einsele, W. Beyer, and U. Rau, "Analysis of sub-stoichiometric hydrogenated silicon oxide films for surface passivation of crystalline silicon solar cells," J. Appl. Phys. **112**, 054905 (2012).

[6]H. Fujiwara, T. Kaneko, and M. Kondo, "Application of hydrogenated amorphous silicon oxide layers to c-Si heterojunction solar cells," Appl. Phys. Lett. **91**, 133508 (2007).

[7]H. Fujiwara and M. Kondo, "Impact of epitaxial growth at the heterointerface of a-Si:H/c-Si solar cells," Appl. Phys. Lett. **90**, 13503 (2007).

[8]J. Sritharathikhun, F. Jiang, S. Miyajima, A. Yamada, and M. Konagai, "Optimization of p-type hydrogenated microcrystalline silicon oxide window layer for high-efficiency crystalline silicon heterojunction solar cells," Jpn. J. Appl. Phys., Part 1 **48**, 101603 (2009).

[9]C. Banerjee, J. Sritharathikhun, A. Yamada, and M. Konagai, "Fabrication of heterojunction solar cells by using microcrystalline hydrogenated silicon oxide film as an emitter," J. Phys. D: Appl. Phys. **41**, 185107 (2008).

[10]K. Ding, U. Aeberhard, F. Finger, and U. Rau, "Silicon heterojunction solar cell with amorphous silicon oxide buffer and microcrystalline silicon oxide contact layers," Phys. Status Solidi (RRL) **6**, 193–195 (2012).

[11]S. Rattanapan, T. Watahiki, S. Miyajima, and M. Konagai, "Improvement of rear surface passivation quality in p-type silicon heterojunction solar cells using boron-doped microcrystalline silicon oxide," Jpn. J. Appl. Phys., Part 1 **50**, 082301 (2011).

[12]F. Einsele, P. J. Rostan, M. B. Schubert, and U. Rau, "Recombination and resistive losses at ZnO/a-Si: H/*c*-Si interfaces in heterojunction back contacts for Si solar cells," J. Appl. Phys. **102**, 94507 (2007).

[13]R. A. Sinton, A. Cuevas, and M. Stuckings, "Quasi-steady-state photoconductance. A new method for solar cell material and device characterization," in *Proceedings of the 25th IEEE Photovoltaic Specialists Conference, Washington DC, USA, 13–17 May 1996* (IEEE, 1996), pp. 457–460.

[14]R. T. Sanderson, *Chemical Bonds and Bond Energy* (Academic Press, New York, 1976).

[15]L. Korte, E. Conrad, H. Angermann, R. Stangl, and M. Schmidt, "Advances in a-Si:H/c-Si heterojunction solar cell fabrication and characterization," Sol. Energy Mater. Sol. Cells **93**, 905–910 (2009).

[16]N. Jensen, R. A. Hausner, R. B. Bergmann, J. H. Werner, and U. Rau, "Optimization and characterization of amorphous/crystalline silicon heterojunction solar cells," Prog. Photovoltaics **10**, 1–13 (2002).

[17]A. Froitzheim, R. Stangl, L. Elstner, M. Kriegel, and W. Fuhs, "AFORS-HET: A computer-program for the simulation of heterojunction solar cells to be distributed for public use," in *Proceedings of the 3rd World Conference on Photovoltaic Energy Conversion, Osaka, Japan, 11-18 May 2003* (WIP, 2003), pp. 279–282.

[18]J. Sritharathikhun, H. Yamamoto, S. Miyajima, A. Yamada, and M. Konagai, "Optimization of amorphous silicon oxide buffer layer for high-efficiency p-type hydrogenated microcrystalline silion oxide/n-type crystalline silicon heterojunction solar cells," Jpn. J. Appl. Phys., Part 1 **47**, 8452–8455 (2008).

[19]S. De Wolf and M. Kondo, "Boron-doped a-Si:H/c-Si interface passivation: Degradation mechanism," Appl. Phys. Lett. **91**, 112109 (2007).